

# The selective ethanol gas sensing performance of $\text{CdO}_{1-x}\text{ZnO}_x$ nanocomposite

A. K. Sharma<sup>1</sup> · S. S. Potdar<sup>1,2</sup> · K. S. Pakhare<sup>3</sup> · B. M. Sargar<sup>3</sup> · M. V. Rokade<sup>4</sup> · N. L. Tarwal<sup>5</sup>

Received: 3 September 2016 / Accepted: 28 October 2016 / Published online: 8 November 2016  
© Springer Science+Business Media New York 2016

**Abstract** The  $(\text{CdO})_{1-x}\text{ZnO}_x$  composite films have been deposited onto the glass substrate by simple and inexpensive chemical bath deposition (CBD) method. In synthesis of composite thin films, 0.1 M  $\text{Cd}(\text{NO}_3)_2$  and 0.1 M  $\text{Zn}(\text{NO}_3)_2$  were used as a sources of cadmium and zinc ions, respectively. Liquor ammonia was added as complexing agent in precursor solution. The XRD patterns of composite samples revealed distinct peaks of ZnO and CdO, which clearly indicates formation of CdO–ZnO nanocomposites in thin film form. SEM micrographs of  $(\text{CdO})_{1-x}\text{ZnO}_x$  samples with  $x = 0.25$  shows nanowire-like morphology grown over the entire glass substrate while the samples with  $x = 0.75$  shows the development of nanoflakes. Spherical granular morphology have been observed for sample with  $x = 0.50$ . Elemental compositions of the all deposited films have been confirmed by EDAX. The gas sensing behavior of the pure and composite sensor was systematically investigated for three

different test gases such as ethanol, ammonia and hydrogen sulfide. Under optimum operating temperature of 275 °C and 24 ppm ethanol, the CdO–ZnO sensor showed maximum response of 58.69% among other test gases. The response and recovery time of CdO–ZnO sensor for ethanol was found to be 54 and 59 s, respectively. The CdO–ZnO composite sensor showed better response than pure ZnO and CdO sensor, which is attributed n–n heterojunction at intergrain boundaries. In addition, the energy band structure of CdO–ZnO heterojunction and the ethanol sensing mechanism are analyzed. The CdO–ZnO sensor is found to be selective towards ethanol even at lower concentration.

## 1 Introduction

The detection and monitoring of number of toxic gases has become very important for environmental safety worldwide. Sensor technology is one of the most important key technologies of the future with a constantly increasing demand with number of applications in the industrial as well as in private sectors. More and more gas sensors are used in controlling the technical processes, in environment monitoring, healthcare, and in food industry. Accordingly, the development of fast and sensitive gas sensors with small cross sensitivity is the subject of intense research [1]. Numerous metal oxides like  $\text{WO}_3$  [2],  $\text{CuO}$  [3],  $\text{SnO}_2$  [4] finds application in gas sensors. Zinc oxide has proven its diverse usage in different fields such as solar cells [5], photocatalyst [6] and gas sensors [7]. Cadmium oxide (CdO) is a well-known II–VI semiconductor with a direct band gap of 2.2–2.5 eV [8]. Cadmium oxide is an oxygen deficient n-type semiconductor and it has various applications such as solar cells [9], photodiode [10] and sensors

✉ S. S. Potdar  
sachinpotdar20@gmail.com

A. K. Sharma  
aks\_phy@unishivaji.ac.in

<sup>1</sup> Earth and Space Science Laboratory, Department of Physics, Shivaji University, Kolhapur 416004, India

<sup>2</sup> Department of Physics, Shree Datta Polytechnic College, Shirol, Tal- Shirol, Dist- Kolhapur 416120, India

<sup>3</sup> Department of Chemistry, Jaysingpur College Jaysingpur, Tal- Shirol, Dist- Kolhapur 416101, India

<sup>4</sup> Semiconductor Laboratory, Centre for Materials for Electronics Technology (C-MET), IDA Phase-III, Cherlapally, HCL (PO), Hyderabad 500051, India

<sup>5</sup> Department of Physics, LalBahadurShastri College, Satara, M.S. 415002, India

[11]. However, ZnO suffers from low conductivity, so need to operate at high operating temperature in gas sensors. On the other hand, toxicity of CdO limits its proficient application in gas sensors. There are several parameters of materials for gas sensor applications, such as adsorption ability, sensitivity, thermodynamic stability, response and recovery time, etc. Different metal oxide materials appear advantageous in some of these properties, but very few of them are favorable in all requirements. To overcome with these drawbacks, fabrication of nanocomposite can be the effective approach for high performance gas sensors. The synergistic effect of nanocomposites can improve the performance of an ultimate application. So, there are several nanocomposites were prepared and studied for various applications such as SnO<sub>2</sub>-ZnO [12, 13], Fe<sub>2</sub>O<sub>3</sub>-ZnO [14], ZnO-CuO [15] etc. Nanocomposites were synthesized by numerous chemical methods. Among the facile chemical deposition methods, Chemical bath deposition (CBD) is advantageous in terms of simple, inexpensive, facile and rapid deposition technique. Also, the preparative parameters are easily controllable.

On the basis of above considerations, in present work we have synthesized CdO-ZnO nanocomposite by CBD method. The influence of composition variation of CdO and ZnO on structural, morphological properties of CdO-ZnO thin films are investigated by means of XRD, SEM, EDAX, etc., analysis. Furthermore, the gas sensing characteristic of the annealed samples was investigated for three test gases (TGs) viz: ethanol, hydrogen sulfide and ammonia. The gas sensitivity measurements were carried out at different operating temperature. The temperature at which the sensitivity is higher is the operating temperature of sensor. At this temperature, the effect of gas concentration is studied. Response and recovery characteristic of sensor was also studied.

## 2 Experimental

In this present work, CdO-ZnO composite synthesized by chemical bath deposition method. Initially, Glass substrates thoroughly washed with distilled water and labogent. Then heated in concentrated chromic acid for 1 h and kept in it for 5 h. Finally the glass substrates were washed with double distilled water and ultrasonically cleaned for 15 min at room temperature. Afterward, 0.1 M Zinc nitrate [Zn(NO<sub>3</sub>)<sub>2</sub>] and 0.1 M Cadmium nitrate [Cd(NO<sub>3</sub>)<sub>2</sub>] were used as source of Zinc and Cadmium ions respectively. For obtaining pure ZnO (or CdO) liquor ammonia was added as complexing agent in precursor solution. Initially milky and turbid precipitate was formed but on addition of excess ammonia dissolves this turbidity. Finally, washed substrates were inserted vertically in above prepared bath at room

temperature until the good fine deposition had been obtained. Composite film of ZnO and CdO were prepared by taking 3:1, 1:1 and 1:3 stoichiometric ratios by maintaining total volume of 100 ml. The above mentioned procedure was followed for making the composite. Samples were named as ZC (for pure ZnO), CC (For pure CdO), C1 (1:3 mixture of CdO:ZnO), C2 (1:1 mixture of CdO:ZnO), C3 (3:1 mixture of CdO:ZnO) bath. Finally all samples had been air dried at room temperature for 3–4 h then subjected for annealing at temperature 450 °C for 2 h in muffle furnace. After cooling samples had taken out and were used for further characterization. To study the structural properties of annealed films, X-ray diffraction patterns were obtained using X-ray diffractometer over 2θ (scanning angle range of 20°–80° with Cu K<sub>α</sub> radiation). The surface morphological studies were carried out with scanning electron microscopy (SEM). Energy dispersive X-ray analysis (EDAX) was employed for the compositional studies. The gas sensing properties of synthesized films were studied using a “static gas-sensing system.” There were electrical feeds through the base plate. The heater was fixed below the base plate to heat the sample under test up to required operating temperatures. Al-Cr thermocouple was used to sense the operating temperature of the sensors. The output of the thermocouple was connected to digital temperature indicators. A gas inlet valve was provided at one port of the base plate. The required gas concentration inside the static system was attained by injecting a known volume of test gas using a gas-injecting syringe. For electrical measurements, silver paste contacts were made on the sample of area 1 cm × 1 cm. Initially, the I-V characteristics were studied within ±10 V and it was found that in the above voltage range, the silver contacts showed ohmic behavior. The electrical resistance of films in air (R<sub>a</sub>) and in the presence of test gas (R<sub>g</sub>) was measured to evaluate the gas response, S, defined as follows:

$$S(\%) = \frac{R_a - R_g}{R_a} \times 100 \quad (1)$$

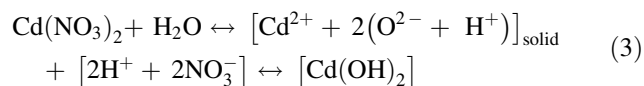
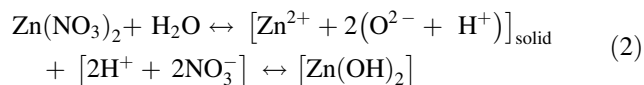
## 3 Results and discussion

### 3.1 Film formation and growth mechanism

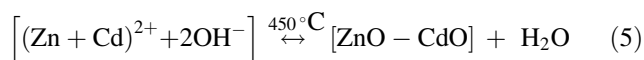
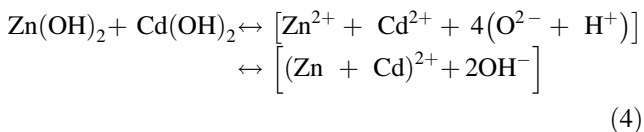
The synthesis of oxides by CBD is based on the formation of solid phase from a solution, which includes two steps as nucleation and particle growth. In the nucleation the clusters of molecules formed undergo rapid decomposition and particles combine to grow up to a certain thickness of the film by heterogeneous reactions at the substrate surface.

In present case, solutions of appropriate concentrations had been prepared and supersaturated by liquor ammonia with continuous stirring. After some specific period (50–100 h) white coloured deposition took place on glass substrate due to heterogeneous reactions at the substrate surface (Step I). Nanoparticles so obtained were further subjected to annealing to remove hydrated water content and for nanoparticle growth (Step II).

#### Step I



#### Step II



### 3.2 XRD analysis

The structural changes and identification of phases of the thin films obtained by CBD are investigated with the help of X-ray diffraction (XRD). The diffracting angle ( $2\theta$ ) is varied between  $20^\circ$  and  $80^\circ$  and the recorded XRD patterns for all the thin films are shown in Fig. 1. Peaks corresponding to the CdO and ZnO structures were observed in composite samples as shown in Fig. 1. XRD patterns for the samples with composition  $x = 0.25, 0.50$  and  $0.75$  exhibit the pattern for mixing of ZnO and CdO. Figure 1 tells us that all the samples are polycrystalline in nature. As per the (JCPDS no. 36-1451) peaks from (101), (102), (002) and (110) planes of ZnO were observed which corresponds to hexagonal structure. XRD pattern obtained from the CdO–ZnO composite structure showed additional peaks from (111), (200), (220) and (311) planes corresponding to cubic CdO (JCPDS no. 05-0640) beside hexagonal ZnO peaks. It is reported that the ionic radius of  $\text{Cd}^{2+}$  and  $\text{Zn}^{2+}$  are 0.095 and 0.074 nm, respectively. As CdO is added to ZnO, the intensity of ZnO peaks decreases. This indicates that the degree of crystallinity is affected by Cd ions which may be added into hexagonal

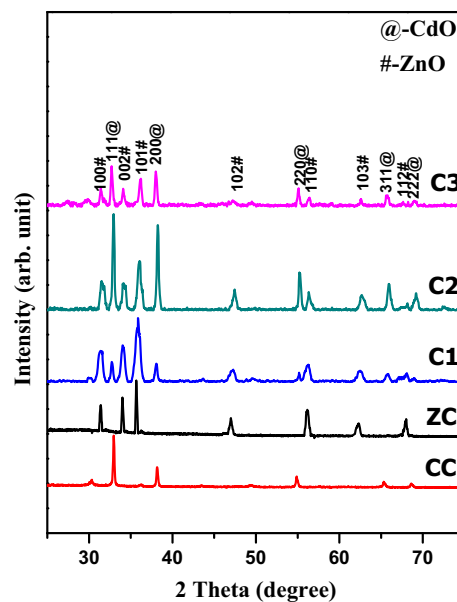


**Fig. 1** Powder X-ray diffraction patterns of CdO (CC), ZnO (ZC),  $\text{ZnO}_{0.25}\text{-CdO}_{0.75}$  (C3),  $\text{ZnO}_{0.50}\text{-CdO}_{0.50}$  (C2),  $\text{ZnO}_{0.75}\text{-CdO}_{0.25}$  (C1)

ZnO structure. The particle size ( $D$ ) is calculated using the following equation,

$$D = 0.9\lambda / \beta \cos \theta \quad (6)$$

where,  $\beta$  is the half width of diffraction peak measured in radian. Calculated particle size for all the annealed samples are tabulated in following Table 1.

### 3.3 Scanning electron microscopy and EDX analysis

SEM micrographs of ZnO, CdO and the composite CdO–ZnO films are shown in Fig. 2a–e and corresponding magnified images are shown in Fig. 2f–j. SEM micrographs of CdO film shows cube-like morphology as shown in Fig. 2a, f while the ZnO shows flower-like morphology, which is shown in Fig. 2b, g. The  $(\text{CdO})_{1-x}\text{ZnO}_x$  samples with  $X = 0.75$  shows development of nanoflakes which grown over complete glass substrate (Fig. 2c, h). Spherical grains observed for samples with  $X = 0.50$  (Fig. 2d, i). Also the samples with  $x = 0.25$  shows the development of

**Table 1** Particle size calculated by using Debye–Scherrer formula

Sr. no.	Sample name	Particle size (nm)
1	C1	14
2	C2	23
3	C3	30
4	ZC	51.4
5	CC	43

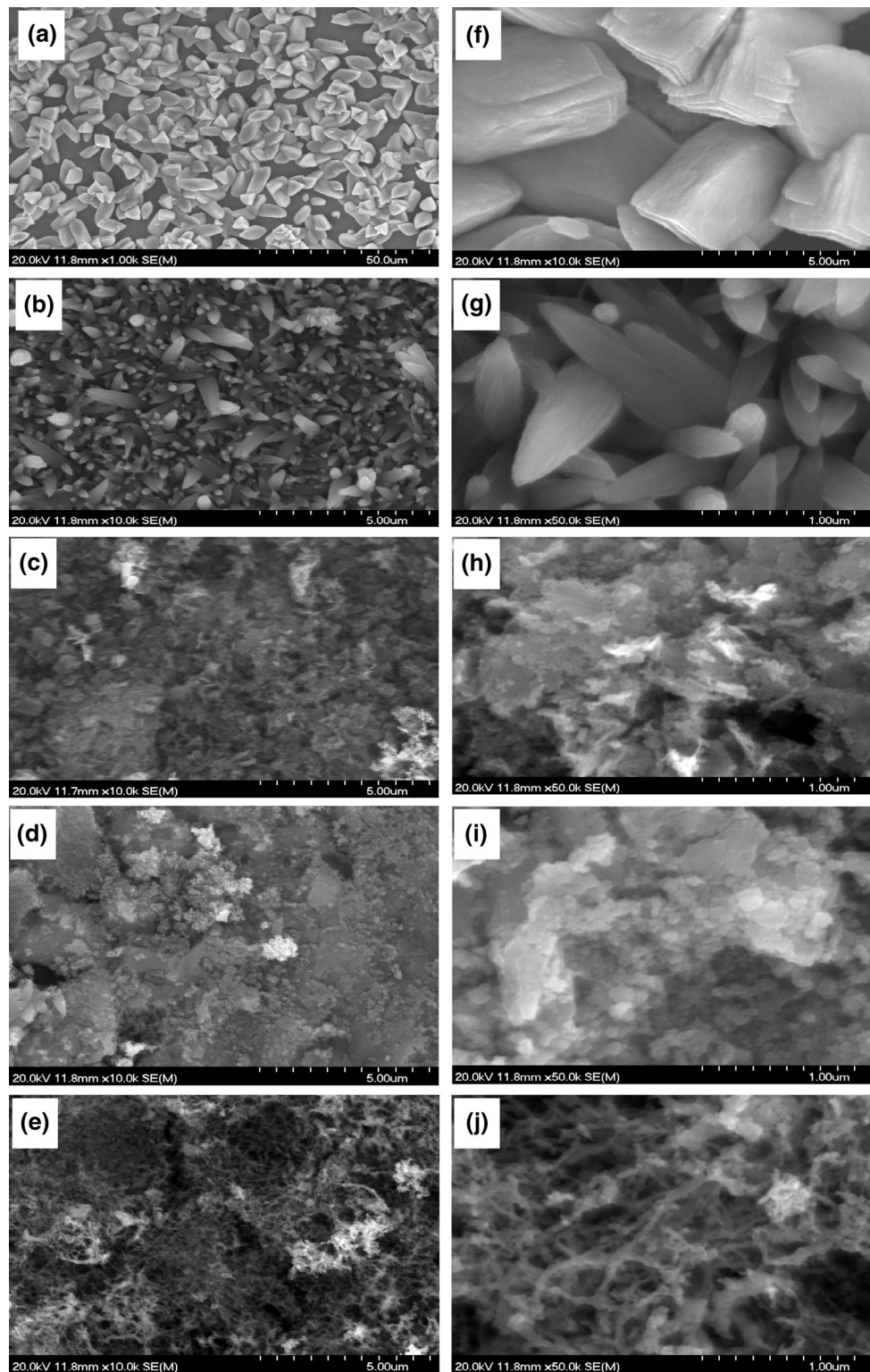


**Fig. 2** Scanning electron microscope images of **a–f** CdO (CC); **b–g** ZnO (ZC), **c–h** Zn<sub>0.75</sub>–Cd<sub>0.25</sub> (C1), **d–i** Zn<sub>0.50</sub>–Cd<sub>0.50</sub> (C2), **e–j** Zn<sub>0.25</sub>–Cd<sub>0.75</sub> (C3) and **f–j** their magnified images, respectively

nanowires (Fig. 2e, f). Such change in morphology creates voids and windows to generate wide porosity. Accordingly we can observe the porosity of the samples increases from

C1 to C3. However, such porous structure is useful in gas sensor application. Elemental composition is confirmed by energy dispersive X-ray analysis. From Fig. 3 and Table 2,

**Fig. 3** EDAX of samples **a** CdO (CC), **b** ZnO (ZC), **c** ZnO<sub>0.25</sub>-CdO<sub>0.75</sub> (C3), **d** ZnO<sub>0.50</sub>-CdO<sub>0.50</sub> (C2), **e** ZnO<sub>0.75</sub>-CdO<sub>0.25</sub> (C1)

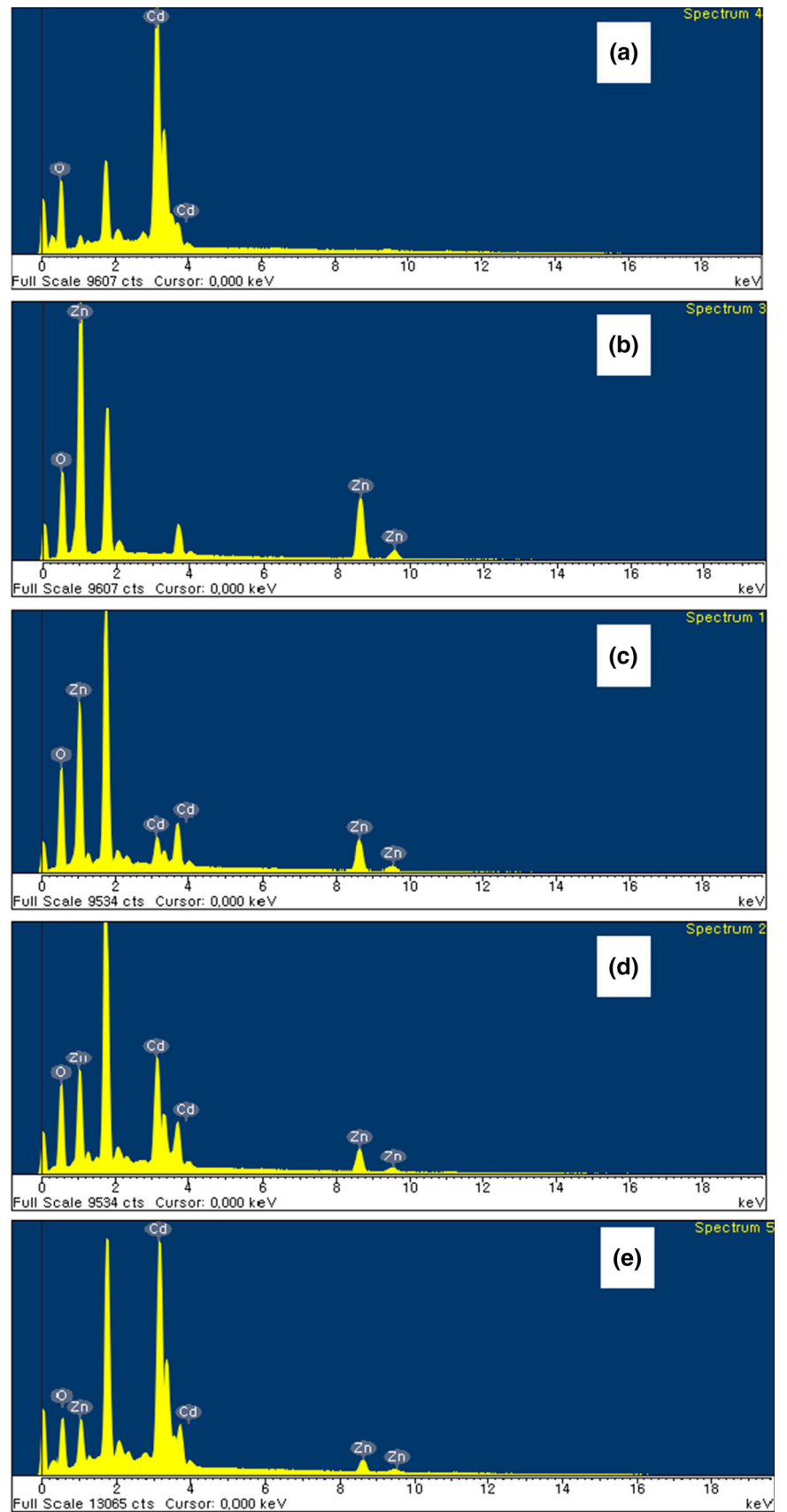


**Table 2** Elemental analysis of sample CC, ZC, C1, C2 and C3 by EDAX

Sample name/element	CC Atomic%	ZC Atomic%	C1 Atomic%	C2 Atomic%	C3 Atomic%
O K	85.35	69.59	84.05	84.87	79.41
Zn K	0	30.41	13.11	7.29	3.82
Cd K	14.65	0	2.84	7.83	16.76
Total	100	100	100	100	100

it is obvious that elemental composition is in good agreement with the stoichiometric ratio of elements we had maintained during experiment.

### 3.4 Gas sensing properties

It is well known that ZnO as well as CdO are two important kinds of fundamental materials and they have been broadly used as gas sensors [11, 16–18]. Furthermore, combining two materials will form heterojunction at the intergrain boundaries, which modifies the electronic transport. Hence, it is necessary to study the sensing properties of CdO–ZnO gas sensor. The temperature of the sensor surface is one of the most influencing parameter. The temperature affects on the physical properties of the semiconductor sensor material such as charge carrier concentration, Debye length, work function etc. The optimum operating temperature for an effective sensor performance corresponds to that where the material is able to catalytically reduce or oxidize the target gas, simultaneously changing the electrical properties of the sensor material. In order to obtain the optimum operating temperature, the samples (ZC, CC, C1, C2 and C3) were exposed to 24 ppm ethanol, hydrogen sulfide (H<sub>2</sub>S) and ammonia (NH<sub>3</sub>) under different temperatures with the interval of 25 °C. It is evident from Fig. 4 that, response of sensor increases at first and reaches its maximum values at the optimum temperature, then decrease clearly with the increasing temperature. Such behavior can be explained by the kinetics and mechanics of gas reaction which occurred on the surface [19]. For low temperatures the sensor response is confined by the speed of chemical reactions. For higher temperature the sensor response is confined by the speed of the diffusion of gas molecules to that surface. The Fig. 4 shows variation of gas response (%) with operating temperature for different samples (ZC, CC, C1, C2 and C3) for three test gases viz: ethanol (C<sub>2</sub>H<sub>5</sub>OH), hydrogen sulfide (H<sub>2</sub>S) and ammonia (NH<sub>3</sub>). It is obvious from Fig. 4 that sample C2 Shows superior gas sensing behavior over other samples and hence used for further studies. The CdO–ZnO sensor exhibits lower operating temperature and higher response, even at lower concentration of target gases which would be credited to formation of n–n heterojunction at intergrain boundaries. n–n heterojunction provides more effective way for

electron transport, which produces more electrons for oxygen adsorption. From Fig. 5 it has been observed that the CdO–ZnO sensor (sample C2) is more sensitive to ethanol gas than other test gases viz: ammonia (NH<sub>3</sub>) and hydrogen sulfide (H<sub>2</sub>S) at operating temperature of 275 °C. At same concentration CdO–ZnO (sample C2) sensor exhibit higher sensitivity to ethanol (58.69%) than that of the ammonia (NH<sub>3</sub>) (34.3%) and hydrogen sulfide (H<sub>2</sub>S) (31%). CdO–ZnO sensor showed selectivity towards ethanol against ammonia and hydrogen sulfide. Furthermore, Fig. 6 indicates that the response of CdO–ZnO sensor to ethanol gas is higher than that of pure ZnO and CdO sensors under the same concentration. For instance, the response of CdO–ZnO sensor (58.69%) is ≈ 3 times higher than that of ZnO sensor (20%) and CdO sensor (18%) to 24 ppm ethanol at operating temperature of 275 °C. Similarly, it is noted from Fig. 7 that the responses increase with increasing concentration of test gases. The response/recovery time is a crucial parameter, used for characterizing sensors. It is defined as the time required to reach 90% of the final change in resistance, after gas is turned ON or OFF, respectively. By careful measurement, the response time and recovery time of CdO–ZnO sensor towards ethanol is 54 and 59 s, respectively. It is better than pure ZnO and CdO.

Mechanism for the gas sensing of n-type semiconducting metal oxide, the typically accepted theory is based on the electron transport between the sensor surface and chemisorbed species that modify the surface conductivity of the sensor [20]. When the sensor is exposed to air, the atmospheric oxygen molecules are adsorbed on the surface of sensor, and then capture electrons from the conduction band to form the chemisorbed oxygen species (O<sub>2</sub><sup>-</sup>, O<sup>-</sup>, O<sup>2-</sup>)

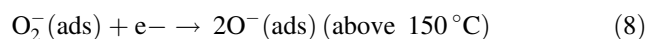
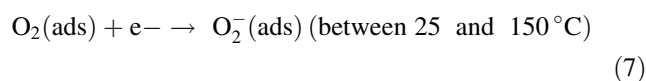
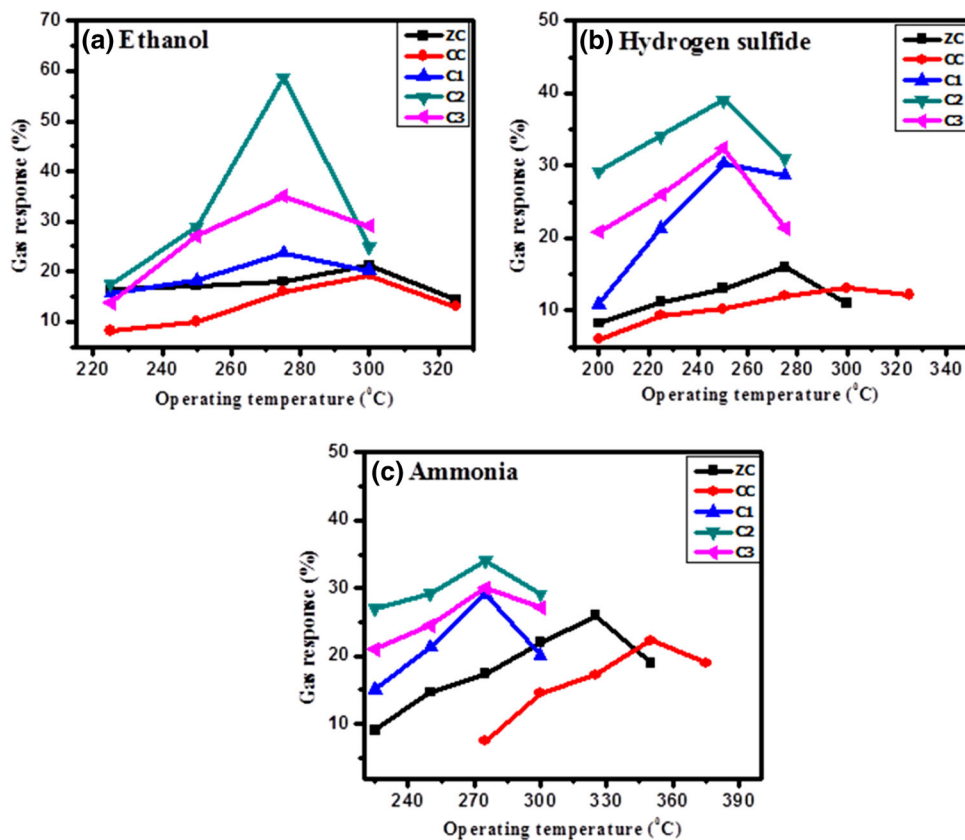
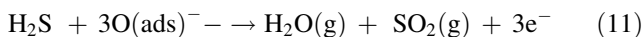
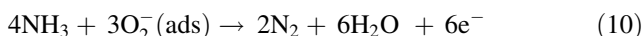


**Fig. 4** Plot of gas response as a function of operating temperature for different samples (ZC, CC, C1, C2, C3) for **a** ethanol, **b** hydrogen sulfide, **c** ammonia to 24 ppm of respective gases

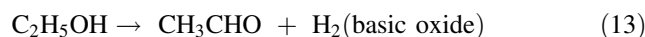
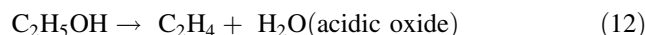


Therefore, the adsorbed oxygen molecules acting as acceptors and thus by deplete the surface electron states and reduce the free carrier density, consequently resulting in the electron depletion region generated at the surface of the sensor.

When the sensor is exposed to target gases (such as ethanol, ammonia and hydrogen sulfide), the reaction between gas molecules and adsorbed oxygen molecules will occur. It releases electrons back to the conduction band of materials. These electrons recombine with holes, which increases the electrical conductivity of the semiconductor. These processes can be described by the following reactions,



In case of ethanol molecules, it may undergo different reaction, i.e., dehydration and dehydrogenation [21].



The intermediate  $\text{CH}_3\text{CHO}$  and  $\text{C}_2\text{H}_4$  can react with oxygen ions to produce  $\text{CO}_2$  and  $\text{H}_2\text{O}$ .



The dehydrogenation reaction is preferred in CdO–ZnO sensor due to basic nature of both CdO and ZnO. These intermediates are helpful for diffusion. It may be noted that the quantity of adsorbed intermediates is more dominant compared with ammonia and hydrogen sulfide. Also the reaction between ethanol and adsorbed oxygen releases the most electrons under the same time span and thus it may cause shorter response time and improved response. The enhanced response as well as lowest working temperature observed in CdO–ZnO sensor as shown in Table 3. Also, the working temperature of CdO–ZnO is the lowest among these materials in Table 3. Recently, many papers have

**Fig. 5** Transient gas response of sample C2 at different operating temperature for **a** ethanol, **b** hydrogen sulfide, **c** ammonia, **d** LPG to 24 ppm of respective gas

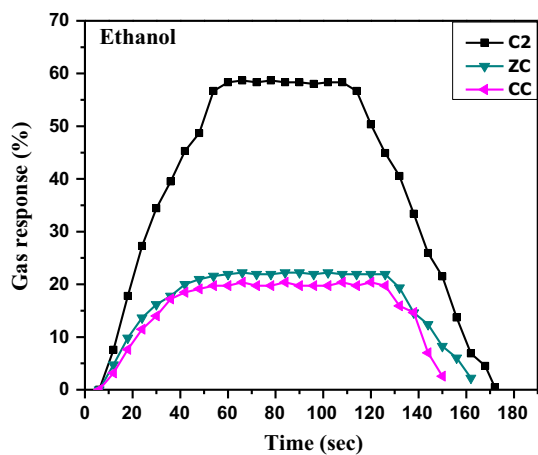
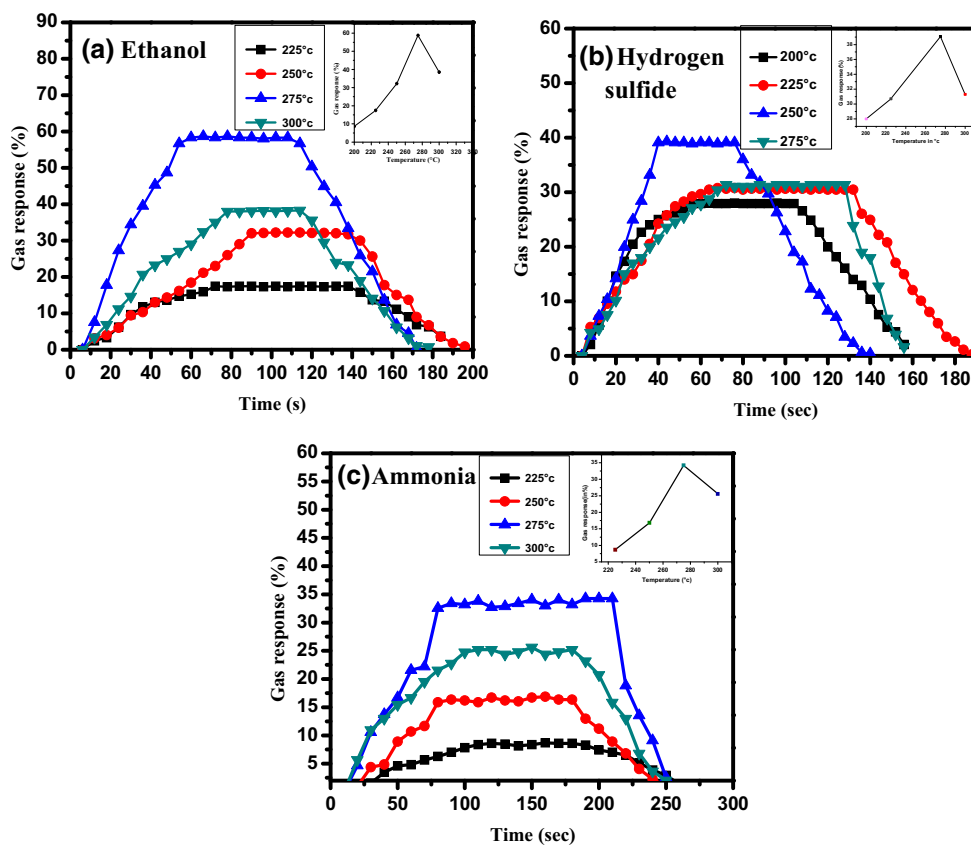


**Fig. 6** Transient gas response of sample C2, ZC and CC at 2750 °C for ethanol to 24 ppm

also suggested that better sensitivity and low working temperature can be obtained from nanocomposites [22–24].

The results cited in Table 3 and the present work propose that nanocomposites are good candidates for gas sensors with high sensitivity and low operating temperature. Such high sensing performance can be credited to the modification of the barrier height at the CdO–ZnO interface. Schematics of energy-level representations of the gas

sensing mechanism of CdO–ZnO heterostructure are shown in Fig. 8. ZnO is the n-type semiconductor with a bandgap of 3.37 eV. CdO is n-type semiconductor with a direct bandgap of 2.3 eV. At the intergrain boundaries between ZnO and CdO, the migration of electrons takes place till Fermi level equalizes. As a result accumulation layer is formed at interface. Whereafter, barrier ( $qV_0$ ) is established at the interface, as shown in Fig. 8a. The resistance is mainly dominated by the height and width of the barrier [28–30]. In air atmosphere, oxygen molecules are absorbed on the surface of both ZnO and CdO and capture electrons from their conduction band to become oxygen ions. The surface band of both ZnO and CdO bends upward and the depletion layer width increases. At the CdO–ZnO interface, the barrier height increases to  $q(V_0 + V_1)$  and the barrier width also increases, as shown in Fig. 8b. Such an increase of barrier height and width would significantly affects on the resistance of system. It has been reported that the resistance is exponentially proportional to the effective barrier height as follows [31].

$$R = R_0 \exp\left(\frac{qv}{kT}\right) \tag{16}$$

After introduction of gas, the surface band of both ZnO and CdO bends downward and the barrier height decreases



**Fig. 7** Response under different gas concentration for **a** ethanol, **b** hydrogen sulfide, **c** ammonia, at their respective operating temperatures

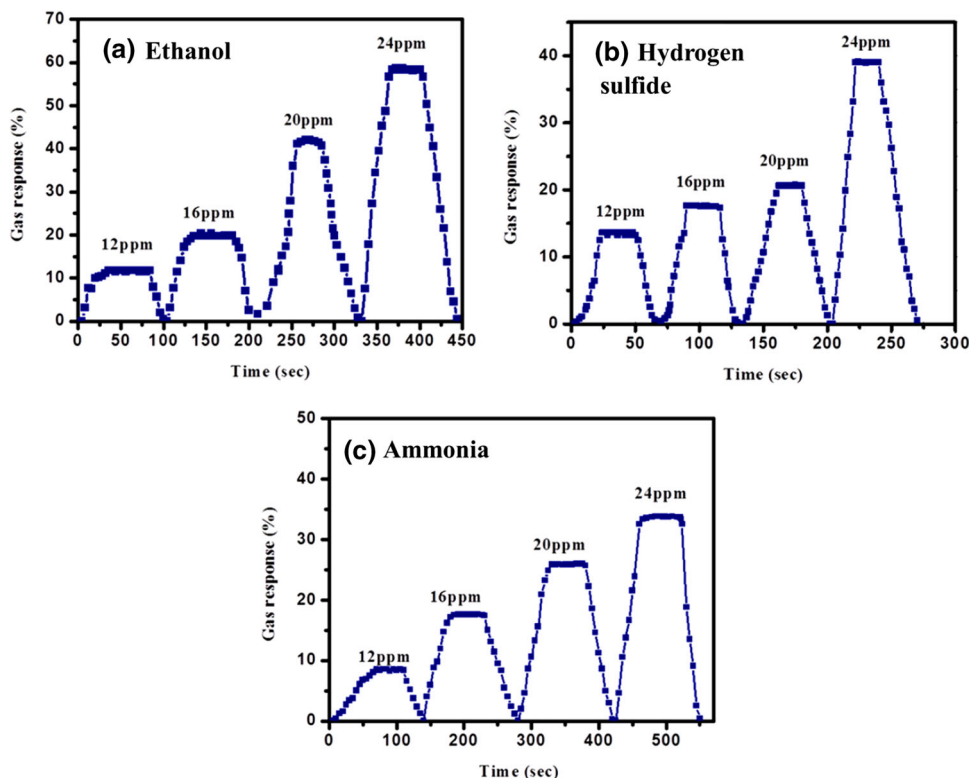
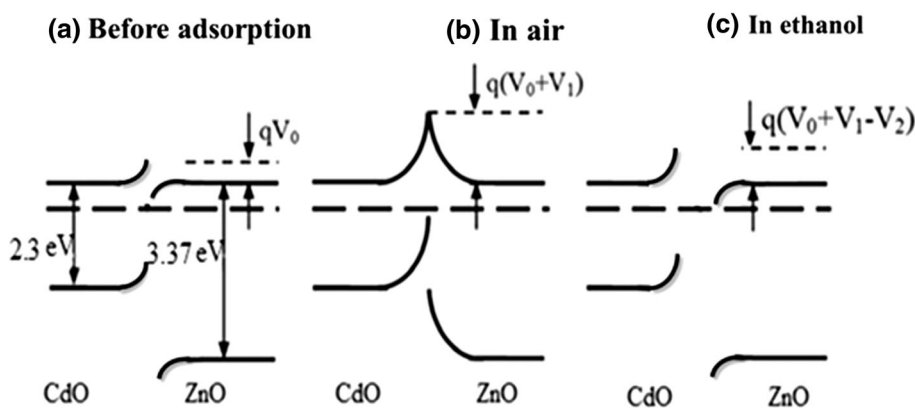


**Table 3** Ethanol sensors based on ZnO materials reported before and CdO–ZnO in present work

Sr. no.	Material	Sensitivity	Concentration (ppm)	Working temperature ( °C)	References
1	ZnO	18.294	100	350	[25]
2	ZnO	7.3	50	–	[26]
3	ZnO	18.9	200	332	[27]
4	CdO–ZnO	58.69	24	275	Present work

**Fig. 8** Schematic and energy level representation of CdO–ZnO heterostructure. **a** Before adsorption, **b** in air, **c** in presence of ethanol



to  $q(V_0 + V_1 - V_2)$ , as shown in Fig. 8c. The resistance of CdO–ZnO sensor decreases significantly and the sensitivity is extremely high. A small change in the barrier height causes the significant change in the resistance of the sensors and thus high reaction temperature is no further

necessary. Thus, the sensitivity of CdO–ZnO sensor is high and the sensors can be operated under low temperature.

## 4 Conclusion

Pure CdO, Pure ZnO and CdO–ZnO nanocomposites were successfully synthesized by chemical bath deposition method. XRD patterns confirmed the phases of ZnO, CdO and their mixed phases. SEM analysis of the samples showed development of nanoflakes and nanowire-like morphology for the composite films with  $X = 0.75$  and  $X = 0.25$ , respectively, while the spherical grains were observed for samples with  $X = 0.50$ . Elemental compositions were confirmed by EDAX analysis. Compared with pure CdO and ZnO sensor, CdO–ZnO composite sensors showed a dramatic improvement in response with shorter response time. Also, the operating temperature is lowered, which is credited to n–n heterojunction at intergrain boundaries. The CdO–ZnO composite sensor showed a maximum response of 58.69% to 24 ppm of ethanol with faster response of 54 s. Thus, CdO–ZnO composite sensor is selective towards ethanol against ammonia and hydrogen sulfide even at lower concentration.

## References

1. A. Khoobi, S.M. Ghoreishi, M. Behpour, M. Shaterian, M. Salavati-Niasari, *Colloids Surf. B Biointerfaces* **123**, 648–656 (2014)
2. M. Stankova, X. Vilanova, E. Llobet, J. Calderer, C. Bittencourt, J. Pireaux, X. Correig, *Sens. Actuators B* **105**, 271–277 (2005)
3. Y.S. Kim, I.S. Hwang, S.J. Kim, C.Y. Lee, *Sens. Actuators B* **135**, 298–303 (2008)
4. N. Barsan, U. Weimar, *J. Phys. Condens. Matter* **15**, 813–839 (2003)
5. D.G. Baik, S.M. Cho, *Thin Solid Films* **354**, 227–231 (1999)
6. M. Nirmala, M.G. Nair, K. Rekha, A. Anukaliani, S.K. Samdarshi, R.G. Nair, *J. Basic Appl. Sci.* **2**(5–6), 161–166 (2010)
7. B. Baruwati, D.K. Kumar, S.V. Manorama, *Sens. Actuators B* **119**, 676–682 (2006)
8. D.M.C. Galicia, R. Castanedo-Perez, O. Jimenez-sandoval, S. Jimenezsandoval, G. Torres-Delgado, C.I. Zuniga-Romero, *Thin Solid Films* **371**, 105–108 (2000)
9. C.H. Champness, C.H. Chan, *Sol. Energy Mater. Sol. Cells* **37**, 75–92 (1995)
10. R. Kondo, H. Okimura, Y. Sakai, *J. Appl. Phys.* **10**, 1547–1554 (1971)
11. R.R. Salunkhe, C.D. Lokhande, *Sens. Actuators B* **129**, 345–351 (2008)
12. J.H. Yu, G.M. Choi, *Sens. Actuators B* **52**, 251–256 (1998)
13. B.P.J. De Lacy Costello, R.J. Ewen, P.R.H. Jones, N.M. Ratcliffe, R.K.M. Wat, *Sens. Actuators B* **61**, 199–207 (1999)
14. C.L. Zhu, Y.J. Chen, R.X. Wang, L.J. Wang, M.S. Cao, X.L. Shi, *Sens. Actuators B* **140**, 185–189 (2009)
15. D.H. Yoon, J.H. Yu, G.M. Choi, *Sens. Actuators B* **46**, 15–23 (1998)
16. R.B. Waghulade, P.P. Patil, R. Pasricha, *Talanta* **72**, 594–599 (2007)
17. V.R. Shinde, T.P. Gujar, C.D. Lokhande, R.S. Mane, S.H. Han, *Sens. Actuators B* **123**, 882–887 (2007)
18. V.R. Shinde, T.P. Gujar, C.D. Lokhande, *Sens. Actuators B* **123**, 701–706 (2007)
19. L. Liu, S. Li, J. Zhuang, L. Wang, J. Zhang, H. Li, *Sens. Actuators B Chem.* **155**, 782–788 (2011)
20. N.L. Tarwal, A.R. Patil, N.S. Harale, A.V. Rajgure, S.S. Suryavanshi, W.R. Bae, P.S. Patil, J.H. Kim, J.H. Jang, *J. Alloys Compd.* **598**, 282–288 (2014)
21. P. Rai, Y.T. Yu, *Sens. Actuators B Chem.* **173**, 58–65 (2012)
22. J.M. Wu, *Nanotechnology* **21**, 235501–235506 (2010)
23. A. Arena, N. Donato, G. Saitta, A. Bonavita, G. Rizzo, G. Neri, *Sens. Actuators B* **145**, 488–494 (2010)
24. M.H. Cao, Y.D. Wang, T. Chen, M. Antonietti, M. Niederberger, *Chem. Mater.* **20**, 5781–5786 (2008)
25. L.J. Bie, X.N. Yan, J. Yin, Y.Q. Duan, Z.H. Yuan, *Sens. Actuators B* **126**, 604–608 (2007)
26. J. Xua, Y. Zhang, Y. Chen, Q. Xiang, Q. Pan, L. Shi, *Mater. Sci. Eng. B* **150**, 55–60 (2008)
27. X. Jiaqiang, C. Yuping, C. Daoyong, S. Jianian, *Sens. Actuators B* **113**, 526–531 (2006)
28. R.M. Lin, M.J. Lai, L.B. Chang, C.H. Huang, *Appl. Phys. Lett.* **97**, 181108-3 (2010)
29. J. Zhou, Y. Gu, Y. Hu, W. Mai, P.H. Yeh, G. Bao, A.K. Sood, D.L. Polla, Z. Wang, *Appl. Phys. Lett.* **94**, 191103-3 (2009)
30. P.H. Yeh, Z. Yeh, Z. Li, Z.L. Wang, *Adv. Mater.* **21**, 4975–4978 (2009)
31. J.Q. Liu, S.P. Gong, Q.Y. Fu, Y. Wang, L. Quan, Z.J. Deng, B. Chen, D.X. Zhou, *Sens. Actuators B* **150**, 330–338 (2010)